Organometallic Chemistry on a Metallathiaborane Cluster: Reactions of [8,8-$(PPh_3)_2$-*nido*-8,7-$RhSB_9H_{10}$] with Bidentate Phosphine Ligands

Ramón Macías, Nigam P. Rath, and Lawrence Barton*

Department of Chemistry, University of Missouri—St. Louis, St. Louis, Missouri 63121

Received February 22, 1999

Reactions of the unsaturated cluster [8,8-$(PPh_3)_2$-*nido*-8,7-$RhSB_9H_{10}$] (**1**) with the bidentate 1,*n*-bis(diphenylphosphino)alkanes $(CH_2)_n(PPh_2)_2$, where $n = 1-3$ (abbreviated as dppm, dppe, and dppp, respectively), have been studied. When a 1:1 molar ratio of phosphine to rhodathiaborane is used, for dppe and dppp, simple substitution to form [8,8-(η^2-dppe)-*nido*-8,7-$RhSB_9H_{10}$] (**2**) or [8,8-(η^2-dppp)-*nido*-8,7-$RhSB_9H_{10}$] (**3**) is observed. However, in the presence of an excess of dppe or dppp, mixtures of the species **2** and [8,8-(η^2-dppe)-9-(η^1-dppe)-*nido*-8,7-$RhSB_9H_{10}$] (**4**) or of **3** and [8,8-(η^2-dppp)-9-(η^1-dppp)-*nido*-8,7-$RhSB_9H_{10}$] (**5**) are formed, respectively. Under both sets of conditions, when dppm is used, only one product, [8,8-(η^2-dppm)-8-(η^1-dppm)-*nido*-8,7-$RhSB_9H_{10}$] (**6**), is observed. This latter species has two dppm ligands coordinating to the metal, one in a unidentate mode and the other bidentate. Species **2** and **3** are formally unsaturated, two electrons short of the number required for the observed 11-vertex *nido* structure. In contrast, **4** and **5** are saturated with the cage-bonded unidentate ligand providing an additional skeletal electron pair to the cluster. The species **4** and **5** are unstable in solution; depending on the conditions, they dissociate to give free phosphine and the chelate **2** or **3** or they undergo *nido* to *closo* transformation with loss of dihydrogen, affording the corresponding 11-vertex *closo* compounds [1,1-(η^2-dppe)-3-(η^1-dppe)-*closo*-1,2-$RhSB_9H_8$] (**17**) and the dppp analogue [1,1-(η^2-dppp)-3-(η^1-dppp)-*closo*-1,2-$RhSB_9H_8$] (**18**). Further reaction in the case of **5** allows isolation of the linked cluster system [{1,1-(η^2-dppp)-*closo*-1,2-$RhSB_9H_8$}$_2$-3,3′-(μ-dppp)] (**19**). The species have been characterized by NMR and mass spectrometry, and crystal structure determinations are described for **3**, the OEt derivative of **3**, [8,8-(η^2-dppp)-9-(OEt)-*nido*-$RhSB_9H_9$] (**14**), **6,** and the phosphine oxide of **17,** [1,1-(η^2-dppe)-3-(η^1-dppeO)-*closo*-1,2-$RhSB_9H_8$] (**20**).

Introduction

The organometallic chemistry of metallacarboranes has been reasonably well-studied during the last 30 years.[1] In contrast, the reactivity of polyhedral metallaboranes and metallaheteroboranes (containing p-block elements other than carbon in the cluster framework) has been less developed. There is great potential for novel chemistry in this latter area, as evidenced by some of the remarkable studies heretofore conducted. For example, the reaction of the iridaborane [6,6-(PPh_3)H-6,5-μ-$(Ph_2P$-*o*-$C_6H_4)$-*nido*-6-IrB_9H_{12}] with acetylene affords [10-(PPh_3)-2,2-$(PH_3)_2$-1,2-μ-$(Ph_2P$-*o*-$C_6H_4)$-*closo*-2-IrB_9H_7] and [1,1,1-$(C_4H_4)(Ph_2P$-*o*-$C_6H_4)$-*isocloso*-1-IrB_9H_7-5-(PPh_3)-2].[2] In the former, the PPh_3 ligands have been converted to PH_3 ligands[2a] and the cluster oxidized from *nido* to *closo*; in the latter, two acetylene groups have been coupled to form an iridacyclopenta-2,4-dienyl moiety and the cluster transformed from *nido* to *closo*.[2b] Other reactions of alkynes and alkenes with metallaboranes in which reaction appears to take place at the metal center have been reported. These include aromatization of norbornadiene at a Rh center[3] and reactions involving metal-promoted alkyne[4a] and norbornadiene[4b] insertion into B−H bonds, although incorporation of carbon into the cluster was not observed in either case. In our laboratory, we have observed that reactions of *arachno*-[$(PMe_3)_2$(CO)IrB_8H_{11}] with acetylenic substrates afford new metallacarboranes as the result of carbon incorporation into the cluster framework.[5,6] Related to these results are reactions of metallaboranes with unsaturated bases such as nitriles, which can form

(1) (a) Grimes, R. N. In *Comprehensive Organometallic Chemistry*; Wilkinson, G., Abel, E. W., Stone, F. G. A., Eds.; Pergamon: Oxford, U.K., 1982; Part 1, Chapter 5.5, pp 459−543. (b) Geiger, W. E., Jr. In *Metal Interactions with Boron Clusters*; Grimes, R. N., Ed.; Plenum: New York, 1982; p 239. (c) Hawthorne, M. F. *Mol. Struct. Energ.* **1986**, *5*, 225. (d) Grimes, R. N. *Chem. Rev.* **1992**, *92*, 251. (e) Saxena, A. K.; Hosmane, N. S. *Chem. Rev.* **1993**, *93*, 1081. (f) Grimes, R. N. In *Comprehensive Organometallic Chemistry II*; Wilkinson, G., Abel, E. W., Stone, F. G. A., Eds.; Pergamon: Oxford, U.K., 1995; Vol. 1, Chapter 9, pp 374−430. (g) Saxena, A. K.; Maguire, J. J.; Hosmane, N. S. *Chem. Rev.* **1997**, *97*, 2421. (h) Hawthorne, M. F. *Advances in Boron Chemistry;* Siebert, W., Ed.; The Royal Society of Chemistry: London, 1997; p 261.

(2) (a) Bould, J.; Brint, P.; Fontaine, X. L. R.; Kennedy, J. D.; Thornton-Pett, M. *J. Chem. Soc., Chem. Commun.* **1989**, 1763. (b) Bould, J.; Brint, P.; Fontaine, X. L. R.; Kennedy, J. D.; Thornton-Pett, M. *J. Chem. Soc., Dalton Trans.* **1993**, 2335.

(3) Speckman, D. M.; Knobler, C. B.; Hawthorne, M. F. *Organometallics* **1985**, *4*, 1692.

(4) (a) Brauers, G.; Dossett, S. J.; Green, M.; Mahon, M. F. *J. Chem. Soc., Chem. Commun.* **1995**, 985. (b) Green, M.; Howard, J. A. K.; James, A. P.; Nunn, C. M.; Stone, F. G. A. *J. Chem. Soc., Dalton Trans.* **1987**, 61.

(5) Bould, J.; Rath, N. P.; Barton, L. *Organometallics* **1996,** *15*, 4916.

(6) Bould, J.; Rath, N. P.; Barton, L.; Kennedy, J. D. *Organometallics* **1998,** *17*, 902.

10.1021/om9901168 CCC: $18.00
Publication on Web 08/08/1999

simple metal[7,8] or cage[8,9] adducts, become incorporated into the cage,[10] or in some cases cause cage contraction.[11] Examples of adduct formation include [6-Cp*-6,9-$(MeNC)_2$-*arachno*-6-(RhB_9H_{11})] and [4-(Cp*)-4-(*endo*-MeNC)-*arachno*-4-IrB_8H_{12}], obtained in the reactions between MeNC and the *nido* species [6-$(Cp^*Rh)B_9H_{13}$][8] and [6-$(Cp^*Ir)B_9H_{13}$],[7] respectively. On the other hand, the reaction between the related species [6,6,6-$(PMe_2Ph)_3$-*nido*-6-OsB_9H_{13}] and ^{t}BuNC affords the 10-vertex *isocloso*-osmaborane [1,1,1-$H(PMe_2Ph)_2$-1-OsB_9H_8-5-(PMe_2Ph)][11] in a cluster contraction process. Heteroatom insertion has been observed in the reaction of a RCN moiety with ruthena- and rhodadecaboranes, although it is not clear whether initial interaction between the base and the metallaborane involves the borane cage or the metal center.[10] Finally, an example of stepwise reduction of MeNC to Me_2NH on a ruthenadecaborane cluster has been reported.[8]

In this context of the organometallic chemistry of metallaboranes and metallaheteroboranes, we decided to extend our work on the reactions of small molecules with metallaboranes[5,6] by exploring the reactivity of unsaturated clusters with bidentate phosphine ligands. The motivation for this project was based on our previous success in the interaction of small metallaboranes with bidentate bases wherein pendant phosphine ligands, which exhibit the potential to form linked clusters, were observed.[12] Two substrates came to mind for such a study: [9,9-$(PPh_3)_2$-*nido*-9,7,8-$RhC_2B_8H_{11}$][13] and [8,8-$(PPh_3)_2$-*nido*-8,7-$RhSB_9H_{10}$] (**1**),[14] compounds which are formally isoelectronic and are two electrons short of the number notionally required to satisfy the polyhedral skeletal electron pair theory.[15] Since our goal was not to focus on metallacarboranes, we selected the latter species. Unlike the rhodacarborane, which is unstable, easily rearranging to a more closed configuration,[13] the rhodathiaborane **1** is stable, is easily prepared, and has been more extensively studied.[14,16−19] There are novel features associated with compound **1**. The unsaturation has been put into question, invoking the presence of two unusual *o*-CH···Rh agostic interactions,[16] and the molecule undergoes interesting fluxional behavior in solution.[14a] Compound **1** is reactive toward both electrophiles and nucleophiles. In particular, the reactions of **1** with Lewis bases L (where L = CO, PMe_2Ph, or CH_3CN) result in either addition of the ligand L to the metal center or addition and substitution, giving rise to species such as [8-L-8,8-$(PPh_3)_2$-*nido*-8,7-$RhSB_9H_{10}$] (where L = CO[14b] or CH_3CN[16]) and [8,8,8-$(PMe_2Ph)_3$-*nido*-8,7-$RhSB_9H_{10}$].[17] Interestingly, [8-(CO)-8,8-$(PPh_3)_2$-*nido*-8,7-$RhSB_9H_{10}$] in refluxing benzene leads to the formation of [1-(CO)-1,3-$(PPh_3)_2$-*closo*-1,2-$RhSB_9H_8$], which when treated with an excess of PMe_2Ph at reflux temperature in benzene affords [1-(CO)-1-(PMe_2Ph)-3-L-*closo*-1,2-$RhSB_9H_{10}$] (where L = PMe_2Ph or PPh_3).[14b] Other reaction patterns such as terminal hydrogen substitution at the 9-position by an OEt group[18] or metal incorporation to form 12-vertex bimetallic species have also been reported.[14b] Herein we report the results of a study of the reactions of **1** with the bidentate 1,*n*-bis(diphenylphosphino)alkanes $(CH_2)_n(PPh_2)_2$, where $n = 1-3$ (abbreviated as dppm, dppe, and dppp, respectively). A minor aspect of this work has appeared in a preliminary communication.[20]

Results and Discussion

Reactions of [8,8-$(PPh_3)_2$-*nido*-8,7-$RhSB_9H_{10}$] (**1**) with the respective bidentate phosphines dppe and dppp in a 1:1 molar ratio in CH_2Cl_2 solvent at ambient temperature afford good yields of the corresponding 11-vertex *nido*-rhodathiaboranes [8,8-(η^2-dppe)-*nido*-8,7-$RhSB_9H_{10}$] (**2**) and [8,8-(η^2-dppp)-*nido*-8,7-$RhSB_9H_{10}$] (**3**) as orange and yellow air-stable solids, respectively (eqs 1 and 2). These compounds are formed by substitution reactions, in which the two PPh_3 ligands in **1** are replaced by the bis(diphenylphosphino)alkanes acting as bidentate chelating ligands.

$$[(PPh_3)_2RhSB_9H_{10}] + \text{dppe} \xrightarrow[\text{room temp}]{CH_2Cl_2} \underset{\mathbf{2}}{[\text{dppeRhSB}_9H_{10}]} + 2PPh_3 \quad (1)$$

$$[(PPh_3)_2RhSB_9H_{10}] + \text{dppp} \xrightarrow[\text{room temp}]{CH_2Cl_2} \underset{\mathbf{3}}{[\text{dpppRhSB}_9H_{10}]} + 2PPh_3 \quad (2)$$

When the reactions of compound **1** with dppe and dppp are carried out in 1:3 metallathiaborane to phosphine molar ratios, compounds **2** and **3** are formed together with the yellow *nido*-rhodathiaboranes [8,8-(η^2-dppe)-9-(η^1-dppe)-*nido*-8,7-$RhSB_9H_{10}$] (**4**) and [8,8-(η^2-dppp)-9-(η^1-dppp)-*nido*-8,7-$RhSB_9H_{10}$] (**5**). The new species, **4** and **5**, are formed by substitution reactions at the metal center and the addition of a second ligand at the 9-position in the cluster. Surprisingly, the reaction of **1** with dppm, in either a 1:1 or 1:3 molar ratio, affords the yellow compound [8,8-(η^2-dppm)-8-(η^1-dppm)-*nido*-8,7-$RhSB_9H_{10}$] (**6**).[20] Compound **6** is formed by substitution of the PPh_3 ligands by dppm and the addition of a second dppm molecule at the rhodium atom. The dppm analogues of **2**−**5** are not observed (eqs

(7) Nestor, K.; Fontaine, X. L. R.; Greenwood, N. N.; Kennedy, J. D.; Thornton-Pett, M. *J. Chem. Soc., Dalton Trans.* **1989**, 1465.
(8) Fontaine, X. L. R.; Greenwood, N. N.; Kennedy, J. D.; MacKinnon, P.; Thornton-Pett, M. *J. Chem. Soc., Dalton Trans.* **1988**, 2809.
(9) Ditzel, E. J.; Fontaine, X. L. R.; Greenwood, N. N.; Kennedy, J. D.; Sisan, Z.; Thornton-Pett, M. *J. Chem. Soc., Chem. Commun.* **1989**, 1762.
(10) Ditzel, E. J.; Fontaine, X. L. R.; Greenwood, N. N.; Kennedy, J. D.; Sisan, Z.; Stibr, B.; Thornton-Pett, M. *J. Chem. Soc., Chem. Commun.* **1990**, 1741.
(11) Coldicott, R. S. In *Current Topics in the Chemistry of Boron*; Kabalka, G. W., Ed.; Special Publication 143; Royal Society of Chemistry: London, 1994; p 297.
(12) Barton, L.; Bould, J.; Fang, H.; Hupp, K.; Rath, N. P.; Gloechkner, C. *J. Am. Chem. Soc.* **1997**, *119*, 631.
(13) Jung, C. W.; Hawthorne, M. F. *J. Am. Chem. Soc.* **1980**, *102*, 3024.
(14) (a) Ferguson, G.; Jennings, M. C.; Lough, A. J.; Coughlan, S.; Spalding, T. R.; Kennedy, J. D.; Fontaine, X. L. R.; Štíbr, B. *J. Chem. Soc., Chem. Commun.* **1990**, 891. (b) Coughlan, S.; Spalding, T. R.; Ferguson, G.; Gallagher, J. F.; Lough, A. J.; Fontaine, X. L. R.; Kennedy, J. D.; Štíbr, B. *J. Chem. Soc., Dalton Trans.* **1992**, 2865.
(15) (a) Williams, R. E. *Adv. Inorg. Chem. Radiochem.* **1976**, *18*, 67. (b) Wade, K. *Adv. Inorg. Chem. Radiochem.* **1976**, *18*, 60. (c) Rudolph, R. W. *Acc. Chem. Res.* **1976**, *9*, 446.
(16) Adams, K. J.; McGrath, T. D.; Rosair, G. M.; Weller, A. S.; Welch, A. J. *J. Organomet. Chem.* **1998**, *550*, 315.
(17) Ferguson, G.; Lough, A. L.; Coughlan, S.; Spalding, T. R. *Acta Crystallogr., Sect. C*: *Cryst. Struct. Commun.* **1992**, *C48*, 440.
(18) Murphy, M.; Spalding, T. R.; Ferguson, G.; Gallagher, J. F. *Acta Crystallogr., Sect. C*: *Cryst. Struct. Commun.* **1992**, *C48*, 638.
(19) Adams, K. J.; McGrath, T. D.; Thomas, R. Ll.; G. M.; Weller, A. S.; Welch, A. J. *J. Organomet. Chem.* **1997**, *527*, 283.
(20) Macías, R.; Rath, N. P.; Barton, L. *Angew. Chem., Int. Ed.* **1999**, *38*, 162.

3−5 are not stoichiometric, they just illustrate the outcome of the reactions). The species **2** is not a new

$$[(PPh_3)_2RhSB_9H_{10}] + 3dppe \xrightarrow[\text{room temp}]{CH_2Cl_2} \underset{\mathbf{2}}{[dppeRhSB_9H_{10}]} + \underset{\mathbf{4}}{[(dppe)_2RhSB_9H_{10}]} \quad (3)$$

$$[(PPh_3)_2RhSB_9H_{10}] + 3dppp \xrightarrow[\text{room temp}]{CH_2Cl_2} \underset{\mathbf{3}}{[dpppRhSB_9H_{10}]} + \underset{\mathbf{5}}{[(dppp)_2RhSB_9H_{10}]} \quad (4)$$

$$[(PPh_3)_2RhSB_9H_{10}] + 3dppm \xrightarrow[\text{room temp}]{CH_2Cl_2} \underset{\mathbf{6}}{[(dppm)_2RhSB_9H_{10}]} \quad (5)$$

compound, having been obtained previously in a different, lower yield, route. Our spectroscopic data for **2** conform with the values reported previously.[16] The new species **3**−**6** were characterized by multinuclear NMR spectroscopy and mass spectrometry, and the structures of compounds **3** and **6** were confirmed by single-crystal X-ray diffraction methods. The NMR spectra for **3** were entirely consistent with the crystallographically determined molecular structure, indicating that the crystal selected represented the bulk material. Unfortunately, we were unable to definitively establish purity for **3**. Isolated as a single species by TLC, with NMR spectra exhibiting only peaks attributable to **3**, it gave unsatisfactory elemental analysis results and the mass spectra, although providing a parent cluster in the correct mass region, were noisy and precluded accurate comparisons with the calculated spectra.

The boron-11 NMR spectrum of **3** at 331 K exhibits four different peaks of relative intensity 3:1:4:1. The overlap of the signals precludes complete assignment of the spectrum; however, $^1H\{^{11}B(\text{selective})\}$ experiments, which relate the cluster ^1H resonances to their directly bonded boron atoms, demonstrate that the ^{11}B and ^1H spectra consist of an overlapped 2:1:1:2:2:1 intensity pattern. The ^{31}P NMR spectrum at 331 K shows a broad signal. In contrast, the ^{11}B and ^1H NMR spectra at 231 K reveal nine different BH resonances, whereas the ^{31}P NMR spectrum gives two doublets of doublets, suggesting an asymmetric structure. The presence of a bridging hydrogen atom in the boron framework is revealed at both high and low temperatures in the proton NMR spectra; the resonance appears in the negative region of the spectra (−2.02 ppm at 231 K and −1.80 ppm at 331 K).

The NMR data for **3** at different temperatures are suggestive of an intramolecular dynamic process, which resembles the fluxional behavior of the analogous rhodathiaboranes **1** and **2**, the isoelectronic platinacarborane [8,8-$(PMe_2Ph)_2$-*nido*-8,7-$PtCB_9H_{11}$] (**7**),[21] and the rhodaazaborane [8,8-$(PPh_3)_2$-*nido*-8,7-$RhNB_9H_{11}$] (**8**).[22] The activation energy, $\Delta G^{\ddagger}$, calculated for **3** at the coalescence temperature of 310 K in the ^{31}P NMR spectrum, is 53 kJ mol^{-1}, between the values of 62 and 46 kJ mol^{-1} reported for **7** and **8**, respectively. A

Scheme 1. Proposed "Switching" and Half-Rotation of the Metal Center above the Open Face of the Heteroborane Fragment in Compounds 1−3, 7, and 8

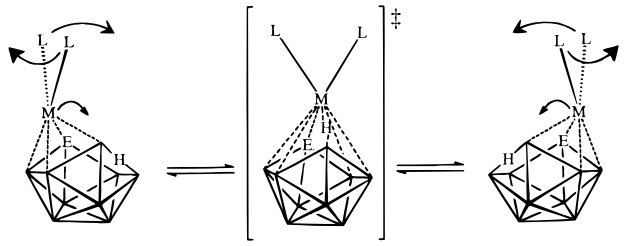

mechanism that may account for the chemical dynamics of this family of isoelectronic 11-vertex metallaheteroboranes has been proposed,[14,21] and it is easily extended to the new species. It involves a shift and rotation of the metal center $\{ML_n\}$ (where M = Rh, L = PPh_3 (**1** and **8**), dppe (**2**), or dppp (**3**); M = Pt, L = PMe_2Ph (**7**)) above the six-membered face {E(7)B(3)B(4)B(9)B(10)B(11)} of the heteroborane fragment $\{EB_9H_{10}\}$ (where E = S (for compounds **1**−**3**), C (for compound **7**), and N (for compound **8**)). In the case of compound **7**, the prochiral nature of the PMe_2Ph phosphine allowed the authors to conclude that the metal center $\{ML_n\}$, rather than a full rotation, undergoes half-rotation (Scheme 1).

The intimate nature of the transition state of this fluxional process is unknown; however, as suggested elsewhere,[21] it is likely to consist of an 11-vertex intermediate of C_s symmetry, with the bridging hydrogen bonded to the metal atom in either a terminal (M−H) or a bridging (M−H−B) fashion. The equilibrium observed in solution between the *nido*-metallacarborane [9,9-$(PEt_3)_2$-9,7,8-$RhC_2B_8H_{11}$] (**9**) and its *isonido* isomer[13] [1,1,1-$H(PEt_3)_2$-1,2,4-$RhC_2B_8H_{10}$] (**10**) and the formation of the *isonido* species [1,1,1-$H(PMe_3)_2$-1,2,4-$IrC_2B_8H_{10}$] (**11**), obtained from the thermolysis of [9,9,9-$CO(PMe_3)_2$-9,7,8-$IrC_2B_8H_{11}$] (**12**),[5a,23] provide chemical support for the proposal of a closed or pseudo-closed species of C_s symmetry as the transition state in the fluxional process described above. This is further suggested by the *nido* to *closo* structural change that compound **2** undergoes upon deprotonation to give the *closo* anion [1,1-(η^2-dppe)-1,2-$RhSB_9H_9]^-$ (**13**), which, upon addition of proton, is reversibly transformed to the parent neutral *nido* compound, **2**.[16,19]

Another perspective of this fluxional process is that there is a continuously reversing internal redox reaction, involving the insertion and extrusion of the metal atom from the B(9)−H−B(10) bond of the heteroborane subcluster $\{EB_9H_{10}\}$ (where E = S (**1**−**3**), C (**7**), and N (**8**)). This would imply a two-electron-oxidation transformation of the metal center $\{M(L_2)\}^+$ upon insertion in the cluster framework to form the oxidized fragment $\{M(L_2)H\}^{2+}$ and two-electron reduction when the metal is extruded. Alternatively, the fluxional behavior of this family of 11-vertex metallaheteroboranes may be simply viewed as a hindered *closo*−*nido* isomerization in solution.

The reaction of **3** with EtOH in CH_2Cl_2−EtOH, in a 1:1 molar ratio, affords the ethoxy derivative [8,8-(η^2-

(21) Štíbr, B.; Jelínek, T.; Kennedy, J. D.; Fontaine, X. L. R.; Thornton-Pett, M. *J. Chem. Soc., Dalton Trans.* **1993**, 1261.
(22) Macías, R. Ph.D. Thesis, University of Leeds, 1996.
(23) Bould, J.; Rath, N.; Barton. L. *Acta Crystallogr., Sect. C*: *Cryst. Struct. Commun.* **1997**, *C53*, 416.

Table 1. Crystal Data and Structure Refinement Parameters for [8,8-(η^2-dppp)-8,7-$RhSB_9H_{10}$] (3), [8,8-(η^2-dppp)-9-(OEt)-8,7-$RhSB_9H_9$] (14), [8,8-(η^2-dppm)-8-(dppm)-8,7-$RhSB_9H_{10}$] (6), and [1,1-(η^2-dppe)-3-(η^1-dppeO)-1,2-$RhSB_9H_8$] (20)

	3	14	6	20
empirical formula	$C_{28}H_{37}B_9Cl_3P_2RhS$	$C_{29}H_{40}B_9OP_2RhS$	$C_{102}H_{114}B_{18}Cl_4P_8Rh_2S_2$	$C_{55}H_{62}B_9OP_4RhS$
fw	774.13	698.81	2210.01	1095.19
temp (K)	218(2) K	223(2)	223(2)	293(2)
wavelength	0.71073	0.71073	0.71073	0.71073
cryst syst	monoclinic	triclinic	triclinic	monoclinic
space group	$P2_1/n$	$P\bar{1}$	$P\bar{1}$	$P2_1/n$
a (Å)	10.8921(1)	10.0168(1)	13.6177(1)	12.6671(1)
b (Å)	16.4904(2)	11.2339(1)	18.8835(2)	21.1004(2)
c (Å)	19.9240(2)	16.2335(2)	22.6213(2)	19.9250(1)
α (deg)	10.8921(1)	75.879(1)	102.61(1)	90
β (deg)	16.4904(2)	74.070(1)	92.675(1)	94.241(1)
γ (deg)	19.9240(2)	74.435(1)	103.587(1)	90
V (Å^3)	3568.76(7)	1663.30(3)	5488.30(9)	5310.99(7)
Z	4	2	2	4
D(calcd) (g/cm^3)	1.441	1.395	1.337	1.370
abs coeff (mm^{-1})	0.872	0.697	0.599	0.522
cryst size (mm)	0.40 × 0.33 × 0.16	0.40 × 0.20 × 0.10	0.33 × 0.26 × 0.18	0.33 × 0.22 × 0.20
F(000)	1568	716	2268	2264
2θ range for data (deg)	1.60−28.30	2.66−55.22	2.24−50	2.82−54
no. of rflns collected	69 334	31 204	60 636	100 986
no. of indep rflns	8440	7340	19 166	11 495
goodness of fit on F^2	1.027	1.063	1.022	1.027
final R indices ($I > 2\sigma(I)$)	R1 = 0.0340	R1 = 0.0409	R1 = 0.0812	R1 = 0.0553
R indices (all data)	wR2 = 0.0925	wR2 = 0.0750	wR2 = 0.2576	wR2 = 0.1565
$(\Delta/\sigma)_{min}$ (e Å^{-3})	−1.008	−0.385	−1.256	−0.529
$(\Delta/\sigma)_{max}$ (e Å^{-3})	1.035	0.390	2.029	1.439

dppp)-9-(OEt)-*nido*-$RhSB_9H_9$] (**14**). The same reactivity is observed for the starting material **1** and for the isoelectronic platinacarborane **7**, which in alcoholic media give the corresponding ethoxy and methoxy species [8,8-(PPh_3)$_2$-9-(OEt)-*nido*-$RhSB_9H_9$] (**15**)[18] and [8,8-(PMe_2Ph)$_2$-9-(OMe)-*nido*-8,7-$PtCB_9H_{10}$] (**16**),[21] respectively. These results indicate that the boron vertex at the 9-position in this series of unsaturated 11-vertex metallaheteroboranes, **1**−**3** and **7**, is prone to undergo nucleophilic substitution reactions of the terminal hydrogen atom.

Compound **14** was characterized by NMR spectroscopy, mass spectrometry, and X-ray diffraction, but we were unable to unambiguously demonstrate purity for this species since the mass spectra were quite noisy, and elemental analysis gave unsatisfactory results. The NMR spectra for **14** were entirely consistent with the crystallographically determined molecular structure, indicating that the crystal selected represented the bulk material. The ^{11}B NMR spectrum consists of nine different resonances; ^{1}H{^{11}B(sel)} experiments indicated the existence of eight terminal hydrogen atoms directly bonded to the corresponding boron atoms of the cluster. The proton NMR spectrum exhibits also the signals of the OEt substituent and the *exo*-polyhedral chelating ligand dppp. In addition, the ^{31}P NMR spectrum at room temperature exhibits two doublets of doublets. In contrast to the parent rhodathiaborane **3**, compound **14** does not feature fluxional behavior even at 373 K, implying, perhaps, $\Delta G^{\ddagger}$ values greater than 64 kJ mol^{-1} for the hypothetical dynamic process in **14**, versus the value of 53 kJ mol^{-1}, found for **3**. An increase in the activation energy upon substitution of the terminal hydrogen atom at the 9-position in the metallaheteroborane cage is also observed in the case of [8,8-(PMe_2-Ph)$_2$-9-(OMe)-*nido*-8,7-$PtCB_9H_{10}$] (**16**), for which the activation energy, $\Delta G^{\ddagger}$, is found to be 12 kJ mol^{-1} greater than that of the unsubstituted parent platinacarborane **7**.[22]

The difference in the activation energy of the substituted versus the unsubstituted species is large, and it may arise from the inductive electron-withdrawing effect (−I, electron acceptance)[24] of the alkoxy substituent at the 9-position, which causes a polarization of the B(9)−H−B(10) bond, suggested by the shift of 1 ppm to low field of the resonance of the bridging hydrogen in **14** with respect that found in **3**. Since this bond participates significantly in the fluxionality described above, it is expected that any change in its electronic character will result in a substantial variation of the energy of the transition state. The differences in the structures of **3** and **14** are minimal except for the B(9)−B(10) distances which differ by 0.083 Å, the OEt derivative distance is 1.944(4) compared to 1.861(5) Å in **3**. This tends to suggest a role for this bond in the fluxional process, although a purely steric influence of the substituent in **14** cannot be ruled out.

The ^{11}B and ^{1}H NMR spectra for **6** indicate the presence of nine BH groups and a B−H−B bridging hydrogen atom. The resonance of the latter is shifted ca. 2 ppm upfield with respect to the values found for **2** and **3**. The ^{31}P NMR spectra, however, suggest two dppm ligands bonded to the rhodium atom, one chelating the Rh atom and the other coordinating in a unidentate mode. The molecular structures of compounds **3**, **14**, and **6** have been confirmed by X-ray analysis and are consistent with their NMR data reported herein. Crystallographic data for the three species are summarized in Table 1, and selected interatomic distances and angles appear in Tables 2−4, respectively. These rhodathiaboranes have an 11-vertex *nido* cluster geometry that can be derived from an icosahedron by removing 1 vertex (Figures 1−3). The sulfur atom is positioned on the open face adjacent to the rhodium center, and in all the species, there is a bridging hydrogen at the open-face B(9)B(10) site. In

(24) Hermánek, S. *Chem. Rev.* **1992**, *92*, 325.

Table 2. Selected Interatomic Distances (Å) and Angles (deg) for [8,8-(η^2-dppp)-8,7-$RhSB_9H_{10}$] (3)

Rh(8)−B(9)	2.138(3)	Rh(8)−B(4)	2.236(3)	Rh(8)−B(3)	2.238(3)
Rh(8)−P(2)	2.2645(6)	Rh(8)−P(1)	2.3324(7)	Rh(8)−S(7)	2.3644(7)
S(7)−B(11)	1.908(4)	S(7)−B(2)	1.984(4)	S(7)−B(3)	2.053(4)
P(2)−C(3)	1.829(3)	B(9)−B(10)	1.861(5))	B(10)−B(11)	1.859(5)
C(1)−C(2)	1.520(4)	C(2)−C(3)	1.532(4)	P(1)−C(1)	1.827(3)
B(9)−Rh(8)−B(4)	49.41(14)	B(4)−Rh(8)−B(3)	46.63(14)	P(2)−Rh(8)−P(1)	91.43(2)
B(9)−Rh(8)−S(7)	93.42(8)	B(3)−Rh(8)−S(7)	52.91(10)	P(1)−Rh(8)−S(7)	90.41(2)
B(11)−S(7)−B(2)	55.61(19)	B(2)−S(7)−B(3)	55.71(16)	B(11)−S(7)−Rh(8)	106.72(11)
B(3)−S(7)−Rh(8)	60.38(9)	C(1)−P(1)−Rh(8)	116.29(9)	C(3)−P(2)−Rh(8)	116.85(9)
B(1)−B(2)−B(3)	57.2(2)	B(11)−B(2)−S(7)	60.10(16)	B(2)−B(3)−S(7)	60.28(16)
B(4)−B(3)−Rh(8)	66.64(15)	B(3)−B(4)−B(1)	59.0(2)	B(3)−B(4)−Rh(8)	66.73(16)
B(9)−B(4)−Rh(8)	62.51(14)	B(9)−B(5)−B(10)	63.3(2)	B(6)−B(5)−B(10)	59.4(2)
B(11)−B(6)−B(10)	64.7(2)	B(6)−B(5)−B(1)	59.6(2)	B(3)−B(1)−B(4)	60.2(2)
B(2)−B(6)−B(1)	60.1(3)	B(5)−B(9)−B(10)	58.6(2)	B(4)−B(9)−Rh(8)	68.08(16)
B(10)−B(9)−Rh(8)	114.17(19)	B(6)−B(10)−B(5)	60.1(2)	B(5)−B(10)−B(9)	58.09(19)
B(11)−B(10)−B(9)	111.1(2)	B(6)−B(11)−B(2)	59.2(3)	B(6)−B(11)−B(10)	58.9(2)
B(10)−B(11)−S(7)	113.0(2)	B(3)−B(2)−S(7)	64.02(16)	S(7)−B(3)−Rh(8)	66.71(11)
P(2)−Rh(8)−S(7)	173.27(3)	C(2)−C(1)−P(1)	112.8(2)	C(2)−C(3)−P(2)	116.4(2)
C(1)−C(2)−C(3)	114.1(2)	B(6)−B(1)−B(5)	60.0(2)	B(1)−B(6)−B(5)	60.4(2)

Table 3. Selected Interatomic Distances (Å) and Angles (deg) for [8-(η^2-dppp)-9-(OEt)-*nido*-8,7-$RhSB_9H_9$] (14)

Rh(8)−B(9)	2.122(3)	Rh(8)−B(4)	2.218(3)	Rh(8)−B(3)	2.264(3)
Rh(8)−P(2)	2.2680(7)	Rh(8)−P(1)	2.3337(8)	Rh(8)−S(7)	2.3693(7)
S(7)−B(11)	1.921(3)	S(7)−B(2)	1.994(4)	S(7)−B(3)	2.064(3)
B(9)−B(10)	1.944(4)	B(9)−O(1)	1.386(3)	O(1)−C(28)	1.436(3)
B(6)−B(11)	1.710(5)	B(10)−B(11)	1.853(5)	C(1)−C(2)	1.533(4)
P(1)−C(1)	1.820(3)	P(2)−C(3)	1.830(3)	C(2)−C(3)	1.531(4)
P(2)−Rh(8)−P(1)	90.08(3)	B(9)−Rh(8)−S(7)	95.98(8)	P(2)−Rh(8)−S(7)	168.43(3)
P(1)−Rh(8)−S(7)	93.60(3)	B(3)−Rh(8)−S(7)	52.85(8)	B(4)−Rh(8)−B(3)	46.47(12)
B(9)−Rh(8)−B(4)	50.91(12)	B(11)−S(7)−Rh(8)	106.02(10)	B(3)−S(7)−Rh(8)	60.95(9)
B(2)−S(7)−B(3)	55.51(14)	B(11)−S(7)−B(2)	57.01(15)	B(6)−B(11)−(10)	580.86(19)
B(10)−B(11)−S(7)	113.14(19)	B(6)−B(11)−B(2)	58.8(2)	B(6)−B(10)−B(5)	60.29(18)
B(5)−B(10)−B(9)	56.03(16)	B(11)−B(10)−(9)	111.9(2)	B(10)−B(9)−Rh(8)	111.06(18)
B(2)−B(6)−B(1)	58.36(19)	B(5)−B(9)−(10)	57.81(17)	B(4)−B(9)−Rh(8)	67.21(14)
B(9)−B(5)−B(10)	66.15(19)	B(5)−B(6)−B(1)	59.88(18)	B(11)−B(6)−(10)	64.6(2)
B(9)−B(4)−Rh(8)	61.88(14)	B(6)−B(5)−B(1)	60.57(18)	B(6)−B(5)−B(10)	58.64(18)
S(7)−B(3)−Rh(8)	66.19(10)	B(3)−B(4)−Rh(8)	68.13(16)	B(3)−B(4)−B(1)	58.73(19)
B(1)−B(2)−B(3)	57.05(18)	B(2)−B(3)−S(7)	60.36(15)	B(4)−B(3)−Rh(8)	65.40(15)
C(1)−P(1)−Rh(8)	111.46(10)	B(3)−B(2)−S(7)	64.13(15)	B(11)−B(2)−S(7)	59.54(15)
C(3)−C(2)−C(1)	115.6(2)	B(3)−B(1)−B(4)	60.39(18)	B(5)−B(1)−B(6)	59.55(17)
C(2)−C(3)−P(2)	117.9(2)	C(3)−P(2)−Rh(8)	117.66(9)	C(2)−C(1)−P(1)	112.25(19)

Table 4. Selected Interatomic Distances (Å) and Angles (deg) for [8,8-(η^2-dppm)-8-(η^1-dppm)-*nido*-8,7-$RhSB_9H_{10}$] (6)

Rh(8)−P(1)	2.393(2)	Rh(8)−P(2)	2.295(2)	Rh(8)−P(3)	2.411(2)
Rh(8)−S(7)	2.370(2)	Rh(8)−B(3)	2.251(10)	Rh(8)−B(4)	2.235(10)
Rh(8)−B(9)	2.280(9)	S(7)−B(2)	2.013(11)	S(7)−B(3)	2.072(10)
S(7)−B(11)	1.908(11)	B(9)−B(10)	1.886(14)	B(11)−B(10)	1.804(17)
B(2)−B(3)	1.893(15)	B(1)−B(2)	1.741(16)		
P(1)−Rh(8)−P(2)	71.30(7)	P(1)−Rh(8)−P(3)	99.12(7)	P(3)−Rh(8)−P(2)	103.44(7)
P(2)−Rh(8)−S(7)	157.25(8)	P(1)−Rh(8)−B(9)	174.4(2)	P(3)−Rh(8)−B(9)	83.5(2)
S(7)−Rh(8)−B(9)	88.2(2)	S(7)−Rh(8)−P(3)	97.24(7)	B(11)−S(7)−Rh(8)	112.0(4)
B(10)−B(9)−Rh(8)	117.7(6)	B(11)−B(10)−(9)	112.1(7)	S(7)−Rh(8)−B(3)	53.2(3)
B(4)−Rh(8)−B(9)	46.7(3)	P(3)−Rh(8)−B(9)	83.5(2)	B(11)−S(7)−B(2)	57.3(5)
B(2)−S(7)−B(3)	55.2(2)	Rh(8)−S(7)−B(3)	60.5(3)	S(7)−B(11)−B(2)	64.2(5)
B(2)−B(11)−B(6)	57.7(6)	B(6)−B(11)−(10)	59.3(7)	B(5)−B(10)−B(6)	58.6(6)
B(6)−B(10)−(11)	59.1(6)	B(5)−B(10)−B(9)	58.4(5)	B(4)−B(9)−Rh(8)	65.3(4)
B(4)−B(9)−B(5)	59.8(6)	B(4)−B(9)−Rh(8)	65.3(4)	B(2)−B(6)−B(11)	64.7(6)
B(1)−B(6)−B(2)	58.9(6)	B(1)−B(6)−B(5)	61.7(6)	B(9)−B(5)−B(10)	63.6(6)
B(1)−B(5)−B(4)	59.9(6)	B(9)−B(5)−B(4)	59.9(5)	B(9)−B(4)−Rh(8)	68.0(4)
B(3)−B(4)−Rh(8)	66.9(5)	B(3)−B(4)−B(1)	58.3(6)	S(7)−B(3)−Rh(8)	66.3(3)
S(7)−B(3)−B(2)	60.8(5)	B(1)−B(3)−B(2)	56.9(6)	S(7)−B(2)−B(3)	64.0(5)
B(1)−B(2)−B(3)	57.4(6)	B(6)−B(2)−B(1)	61.2(7)	B(2)−B(1)−B(3)	65.7

contrast with compounds **1**−**3** and **14**, the structure determination confirms that the rhodium atom in the dppm derivative **6** bears two *exo*-polyhedral ligands, featuring two coordination modes, chelating bidentate and unidentate. The structural parameters for the three clusters are very similar and are within the range found for compounds **1** and **2**. The longest interboron distances are the B(9)−B(10) edge, bridged by a hydrogen atom for compounds **1**, **3**, and **14**, and the B(2)−B(3) edge, flanked by the sulfur atom, for **6**. In all of the compounds **1**−**3**, **6**, and **14** the P−Rh bond distance of the phosphorus atom trans to the sulfur vertex of the cluster is substantially shorter than the other P−Rh bond, trans to the boron side of the cage. The P(1)−Rh(8)−P(2) angles vary from the value of 98.50(2)° in **1**, through 84.22(6), 91.43(2), and 90.08(3)° found in **2**, **3**, and **14**,

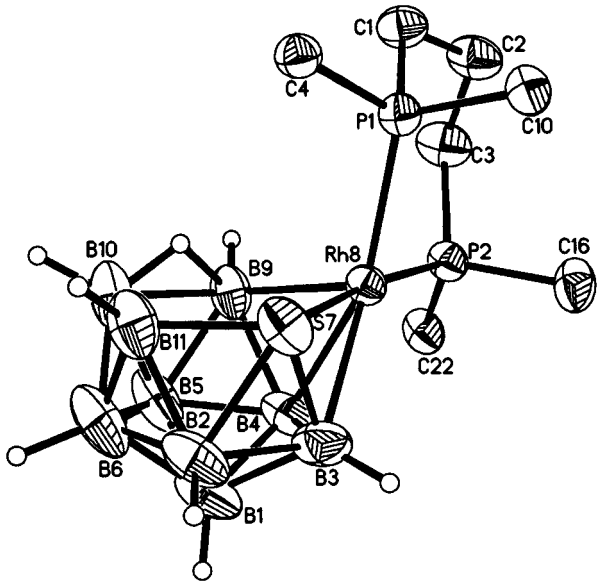

Figure 1. Molecular structure of [8,8-(η^2-dppp)-*nido*-8,7-$RhSB_9H_{10}$] (**3**). Displacement ellipsoids are drawn at the 50% level. The phenyl rings, *ipso*-carbon atoms excepted, are omitted.

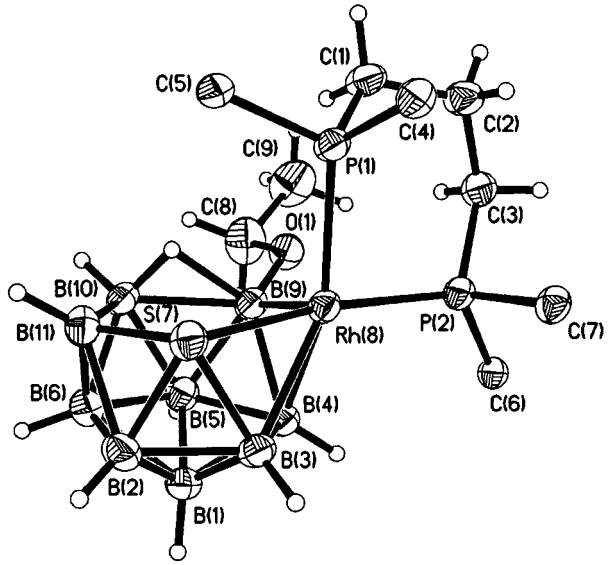

Figure 2. Molecular structure of [8,8-(η^2-dppp)-9-(OEt)-*nido*-8,7-$RhSB_9H_9$] (**14**). Displacement ellipsoids are drawn at the 50% level. The phenyl rings, *ipso*-carbon atoms excepted, are omitted.

respectively, to the value of 71.30(7)° in **6**. A common structural feature of these species is that they exhibit a significant twist of the plane formed by the P(1)Rh(8)P(2) atoms with respect to the plane formed by S(7)Rh(8)B(9). These angles range from the value of 77° found in **2** and **14**, through 59° in **1** and **3**, to 19° in **6**. The large twist angles found for **2** and **14** could be due to exigencies of the chelating ligands and/or packing forces. In the context of the fluxionalty discussed herein, the observed solid-state conformations could also represent rotamers of minimum energy. Compound **6**, in contrast, has a rigid metal-to-thiaborane interaction, in which the chelating dppm ligand is forced to stay almost parallel to the S(7)Rh(8)B(9) plane and the second, monodentate, dppm group completes the coordination sphere around the rhodium atom.

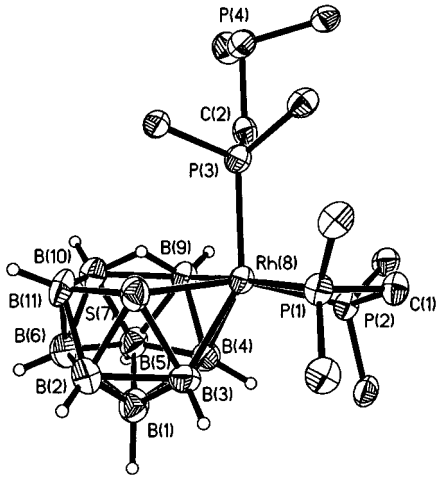

Figure 3. Molecular structure of [8,8-(η^2-dppm)-8-(η^1-dppm)-*nido*-8,7-$RhSB_9H_{10}$] (**6**). Displacement ellipsoids are drawn at the 50% level. The phenyl rings, *ipso*-carbon atoms excepted, are omitted.

Although compounds **1**−**3**, **6**, and **14** have the same basic 11-vertex *nido* structure, their electronic structures, in principle, are different. Compounds **1**−**3** and **14** (and also the isoelectronic **7** and **8**) do not conform to the skeletal electron counting rules, being two electrons short for the observed *nido* structure.[15] This cluster unsaturation can be related to the unsaturated character of the metal vertex,[25] which contributes two orbitals and one electron to the metal-to-thiaborane bonding. In contrast, in compound **6** the rhodium atom is saturated, and the cluster has the predicted number of skeletal electron pairs. Therefore, in terms of a metal-to-ligand description, the unsaturated species can be regarded as "square-planar" 16-electron rhodium complexes, in which 2 coordination positions are occupied by the *exo*-polyhedral groups and the other 2 by the thiaborane fragment, acting as a bidentate ligand in a η^4 fashion. On the other hand, compound **6** resembles an "octahedral" 18-electron complex with 3 coordination positions filled by the two dppm ligands and the other 3 by the thiaborane fragment, acting as a tridentate ligand in a η^4 manner. There is an alternative proposal for the electronic structure of the metal center in compounds related to **1**, **3**, and **14**. Welch and coworkers, in a discussion of compound **2** in another context, have suggested that the Rh atom gains the two electrons via unique agostic interactions between pairs of *ortho* hydrogen atoms on the *P*-phenyl groups, as we described in the Introduction.[16] We prefer to regard these systems as unsaturated. Although the closest C−H···Rh distances in **3** and **14** are all about 3.00 Å, within the ranges described by Welch et al., some B−H···Rh distances are shorter than those for what would be the agostic C−H moieties. We believe that the many examples of square-planar 16-electron metal centers with short electron counts in the literature mitigate against requiring such agostic interactions in **3** and **14**, although we cannot rule them out.

The species **4** and **5**, isolated from the reactions of **1** with excesses of dppe and dppp, respectively (eqs 3 and

(25) (a) Kennedy, J. D. *Main Group Metal Chem.* **1989**, *12*, 149. (b) Barton, L.; Bould, J.; Rath, N. P.; Fang, H. *Inorg. Chem.* **1996**, *35*, 2062. (c) Bould, J.; Cooke, P. A.; Dörfler, U.; Kennedy, J. D.; Barton, L.; Rath, N. P.; Thornton-Pett, M. *Inorg. Chim. Acta*, in press.

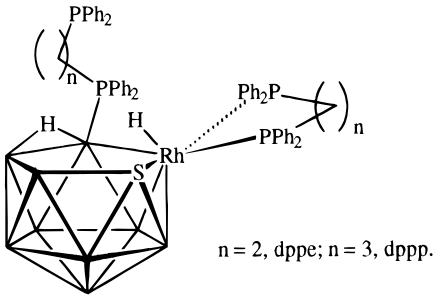

Figure 4. Proposed molecular structure for [8,8-(η^2-dppe)-9-(η^1-dppe)-*nido*-8,7-$RhSB_9H_{10}$] (**4**) and [8,8-(η^2-dppp)-9-(η^1-dppp)-*nido*-8,7-$RhSB_9H_{10}$] (**5**).

4), were characterized by NMR spectroscopy and mass spectrometry. The ^{11}B NMR spectra consist of five broad peaks of relative intensity 1:1:4:2:1 for compound **4** and seven peaks of relative intensity 2:1:1:1:1:2:1 for compound **5**. ^{1}H{^{11}B(sel)} experiments assigned eight different terminal hydrogen atoms to their directly bound boron atoms, indirectly resolving the boron-11 spectra. One of the boron atoms has no terminal hydrogen atom, since it bears a PPh_2 terminus of the 1,*n*-bis(diphenylphosphino)alkane substituent. The ^{1}H NMR spectra include peaks at −1.39 and −11.97 ppm for **4** and at −2.39 and −11.96 ppm for **5**. The signals at the highest frequencies in the negative region of the spectra, which are broad singlets, are assigned to B−B bridging hydrogen atoms on the cluster, whereas the peaks at the lowest frequencies, observed as multiplets, are assigned to the rhodium-bonded hydrides. The ^{103}Rh−^{1}H coupling is clearly visible. The proton NMR spectra also confirm the presence of two *exo*-polyhedral phosphine ligands in both **4** and **5**. Additionally, the ^{31}P NMR spectrum of **4** shows (a) doublets at 59.1 and 54.7 ppm, assigned to the phosphorus atoms of the chelating dppe ligand bound to the rhodium atom, (b) a very broad signal at 5.9 ppm, due to the phosphorus atom directly bonded to a cage boron atom, and (c) a sharp doublet at −12.4 ppm, arising from the pendant PPh_2 group. Similarly, the ^{31}P NMR spectra for **5** exhibit (a) doublets at 13.9 and 9.3 ppm, arising from the chelating dppp ligand, (b) a very broad signal at 7.4 ppm, due to the phosphorus linked to a boron atom, and (c) a sharp singlet at −18.8 ppm, assigned to the pendant phosphine. The observed spectroscopic data suggest that the molecular structures of **4** and **5** are based on 11-vertex *nido* clusters with the rhodium and sulfur atoms adjacent on the pentagonal open face, on which the B(9)−B(10) edge is bridged by a hydrogen atom and a terminal hydride ligand is bonded to the rhodium. The structure is completed by two *exo*-polyhedral bis(diphenylphosphino)alkane groups, one bound in a unidentate manner to the boron atom at the 9-position and the other acting as a chelating ligand at the rhodium center (Figure 4). Mass spectrometry shows the isotopic envelope of the protonated species $[(MO - H_2) + H]^+$ ion at 1054.2 amu for **4** and the $[M]^+$ and $[M + O]^+$ ions at 1067.2 and 1082.4 amu, respectively, for **5**. The mass envelopes for the measured masses for **4** and **5** match those calculated from the known isotopic abundances of the constituent elements. These spectrometric results are consistent with the proposed chemical formulations of **4** and **5** and demonstrate the facile oxygenation of the pendant PPh_2 group present in both species.

The formation of **4** and **5** from the starting material **1** implies (a) substitution of the PPh_3 groups by a chelating bis(diphenylphosphino)alkane ligand at the rhodium atom and (b) nucleophilic attack of a second phosphine at the boron atom at the 9-position, with the concomitant migration of the terminal 9-hydrogen atom to either the B(9)−B(10) bridging position or to the rhodium atom. However, we cannot rule out a mechanism with an initial step similar to the formation of **6**, in which two ligands first coordinate to the metal followed by transfer of the unidentate one to the electrophilic site at B(9). There is no experimental evidence for this process, but it is clear that for the more nucleophilic pendant PPh_2 group on dppp or dppe, it would be sterically more favorable for a concerted transfer of a ligand from Rh to the B(9) position than for dppm. We have no explanation for the absence of the formation of a species involving a bidentate dppm, only, coordinating to the Rh atom, as we observe for **2** and **3**. For descriptive purposes, compounds **4** and **5** can be regarded as phosphine adducts of the unsaturated parent rhodathiaboranes **2** and **3**, respectively. The new adducts have two skeletal electrons more than the parent, conforming therefore to the electron-counting rules.[15]

Interestingly, compounds **4** and **5** are unstable in solution. If a dilute solution of **4** is heated at reflux temperature in CH_2Cl_2 for 1 day, the resultant solution contains a mixture of the parent rhodathiaborane **2** and free phosphine dppe as major components, together with a new species, **17**, as minor component. Under the same conditions, compound **5** affords a mixture of only the parent **3** and free phosphine dppp. In contrast, when a concentrated solution of **4** in $CDCl_3$ is heated at 40 °C in an NMR tube, the new species **17** is obtained almost quantitatively. Under the same conditions, **5** gives a mixture of **3** and free dppp, this time as minor products, and two new compounds, **18** and **19**.

The new compounds were characterized as [1,1-(η^2-dppe)-3-(η^1-dppe)-*closo*-1,2-$RhSB_9H_8$] (**17**), [1,1-(η^2-dppp)-3-(η^1-dpppO)-*closo*-1,2-$RhSB_9H_8$] (**18**), and [{1,1-(η^2-dppp)-*closo*-1,2-$RhSB_9H_8$}$_2$-3,3′-(μ-dppp)] (**19**). The ^{11}B NMR spectra of the three species are almost identical, consisting of five resonances of relative intensity 1:1:3:2:2. ^{1}H{^{11}B(sel)} experiments indicate eight terminal hydrogen atoms in a 1:1:2:1:2:2 relative intensity pattern, which indirectly also resolves the ^{11}B spectra. The ^{31}P NMR spectra are diagnostic of the molecular structures of these compounds. For compounds **17** and **18**, the following signals are found: (a) a sharp doublet in the region corresponding to the chelating phosphine ligands, (b) a doublet and a singlet due to the dangling PPh_2 groups, for **17** and **18**, respectively, and (c) a broad signal for the phosphorus atom bound to a boron atom of the cage. The ^{31}P NMR spectrum of **19** exhibits a doublet, assigned to a dppp chelating ligand, and a very broad signal typical of a phosphorus atom directly bonded to boron; the two signals appear in a 2:1 relative intensity ratio, respectively. In contrast to the ^{31}P NMR spectra of **17** and **18**, compound **19** does not exhibit signals corresponding to either dangling PPh_2 or PPh_2O groups. These spectroscopic results, together with the X-ray analysis of **20**, discussed below, lead us to proposed the molecular structure of **19** as two 11-vertex

Table 5. Selected Interatomic Distances (Å) and Angles (deg) for [1,1-(η^2-dppe)-3-(η^1-dppeO)-*closo*-1,2-$RhSB_9H_8$] (20)

Rh(1)−P(1)	2.2805(12)	Rh(1)−P(2)	2.2638(11)	Rh(1)−S(2)	2.3689(11)
Rh(1)−B(3)	2.106(4)	Rh(1)−B(4)	2.526(5)	Rh(1)−B(6)	2.337(5)
Rh(1)−B(7)	2.437(5)	S(2)−B(4)	1.916(5)	S(2)−B(5)	1.957(6)
S(2)−B(8)	1.999(6)	C(1)−C(2)	1.502(6)	C(27)−C(28)	1.524(5)
B(3)−P(3)	1.920(5)	P(4)−O(1)	1.513(3)	P(3)−C(27)	1.822(4)
P(4)−C(28)	1.822(4)	B(3)−B(6)	1.712(8)	B(4)−B(7)	1.843(7)
P(1)−Rh(1)−P(2)	84.77(4)	P(1)−Rh(1)−S(2)	110.20(5)	P(1)−Rh(1)−B(3)	111.09(14)
P(2)−Rh(1)−B(3)	114.09(13)	P(2)−Rh(1)−S(2)	111.79(4)	S(2)−Rh(1)−B(4)	45.94(12)
S(2)−Rh(1)−B(5)	48.8(2)	B(3)−Rh(1)−B(7)	43.1(2)	B(3)−Rh(1)−B(6)	45.0(2)
Rh(1)−S(2)−B(4)	71.4(2)	Rh(1)−S(2)−B(5)	65.6(2)	B(4)−S(2)−B(8)	58.4(3)
Rh(1)−B(3)−B(7)	78.9(2)	Rh(1)−B(3)−B(6)	74.7(2)	B(7)−B(3)−B(9)	63.8(3)
B(6)−B(3)−B(9)	62.8(3)	P(3)−B(3)−Rh(1)	129.9(2)	Rh(1)−B(4)−S(2)	62.7(2)
Rh(1)−B(4)−B(7)	65.7(2)	B(8)−B(4)−S(2)	63.0(3)	S(2)−B(5)−Rh(1)	65.6(2)
B(6)−B(5)−Rh(1)	65.9(2)	S(2)−B(5)−B(8)	62.3(3)	B(6)−B(5)−B(11)	59.2(3)
B(5)−B(6)−Rh(1)	67.8(2)	B(3)−B(6)−Rh(1)	60.3(2)	B(3)−B(6)−B(9)	59.3(4)
B(3)−B(7)−Rh(1)	58.0(2)	B(4)−B(7)−Rh(1)	70.8(2)	B(4)−B(7)−B(10)	58.4(3)
S(2)−B(8)−B(4)	58.6(2)	Rh(1)−P(1)−C(1)	108.8(2)	C(2)−C(1)−P(1)	108.7(3)
P(2)−C(2)−C(1)	112.4(3)	Rh(1)−P(2)−C(2)	109.8(2)	B(3)−P(3)−C(27)	111.0(2)

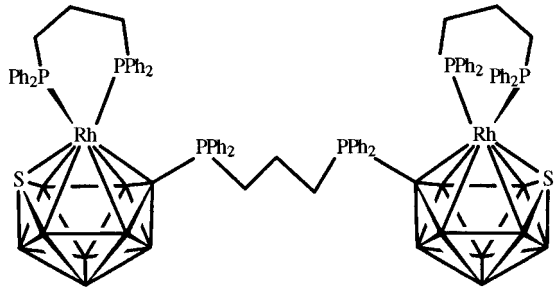

Figure 5. Proposed molecular structure for [{1,1-(η^2-dppp)-*closo*-1,2-$RhSB_9H_8$}$_2$-3,3′-(μ-dppp)] (**19**).

closo clusters linked by an inter-cage bridging dppp ligand (Figure 5). This hypothesis is supported by mass spectrometry, which shows a molecular ion, $[M]^+$, centered at 1718.9 amu, with an isotopic distribution that conforms to the calculated values for the proposed formulation of **19**.

The proposed molecular structures of **17** and **18** are supported by the X-ray diffraction analysis of a crystal of [1,1-(η^2-dppe)-3-(η^1-dppeO)-*closo*-1,2-$RhSB_9H_8$] (**20**). This structure determination also supports the proposed linked-dicage structure of **19**. Crystallographic data for **20** are summarized in Table 1, and selected interatomic distances and angles appear in Table 5. The molecule can be described as an 11-vertex *closo*-rhodathiaborane with the metal center at position 1, which has a connectivity of 6, and the sulfur atoms at the adjacent 2-position (Figure 6). The coordination sphere of the rhodium atom is completed by a bidentate dppe ligand, while a second dppe is linked to B(3); the pendant PPh_2 group bears an oxygen atom, demonstrating that in these species the pendant phosphine group is easily oxidized in the presence of air. The cluster dimensions of **20** are comparable to those of the analogue [1-(CO)-1,3-(PMe_2Ph)$_2$-*closo*-1,2-$RhSB_9H_8$] (**21**),[15] although the latter is reported to exhibit positional disorder of the rhodium atoms. In both *closo*-species the Rh(1)−B(3) distance is ca. 0.2 Å shorter than the distances of Rh(8) with B(4), B(5), B(6) and B(7). The P(3)−B(3) bond length of 1.920(5) Å is within the range 1.87−1.93 Å, usually found for that type of interaction.[26] The conformations of the chelating dppe and dangling and dppeO

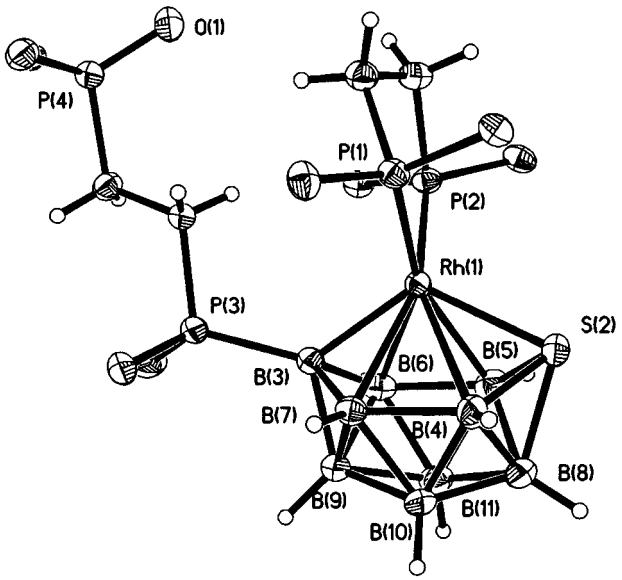

Figure 6. Molecular structure of [1,1-(η^2-dppe)-3-(η^1-dppeO)-*closo*-1,2-$RhSB_9H_8$] (**20**). Displacement ellipsoids are drawn at the 50% level. The phenyl rings, *ipso*-carbon atoms excepted, are omitted.

ligands break the symmetry of the molecule in the solid state; however, fast conformational changes result in an effective C_s point group symmetry in solution.

Conclusions

The reactions of [$(CH_2)_nPPh_2$] (where $n = 1$, dppm; $n = 2$, dppe; $n = 3$, dppp) with **1** have demonstrated that this rhodathiaborane contains two main centers of reactivity: (a) the rhodium atom and (b) the boron atom at the 9-position. The rhodium center behaves as a typical 16-electron complex, undergoing facile substitution of the PPh_3 groups by the chelating bis(diphenylphosphino)alkane ligands. In the case of dppm, a second phosphine molecule is added at the metal center, even if the reaction is carried out in a 1:1 molar ratio. In contrast, an excess of dppe or dppp appears to give rise to nucleophilic attack at the boron atom in the 9-position, although as we point out above, we cannot rule out alternative mechanisms. The resulting P−B bond is labile, and in dilute solutions it dissociates to give a mixture of the corresponding free phosphines and

(26) Kennedy, J. D. *Prog. Inorg. Chem.* **1984**, *32*, 519; **1986**, *34*, 211 and references therein.

Scheme 2. Reactivity of 1 with dppm, dppe, and dppp

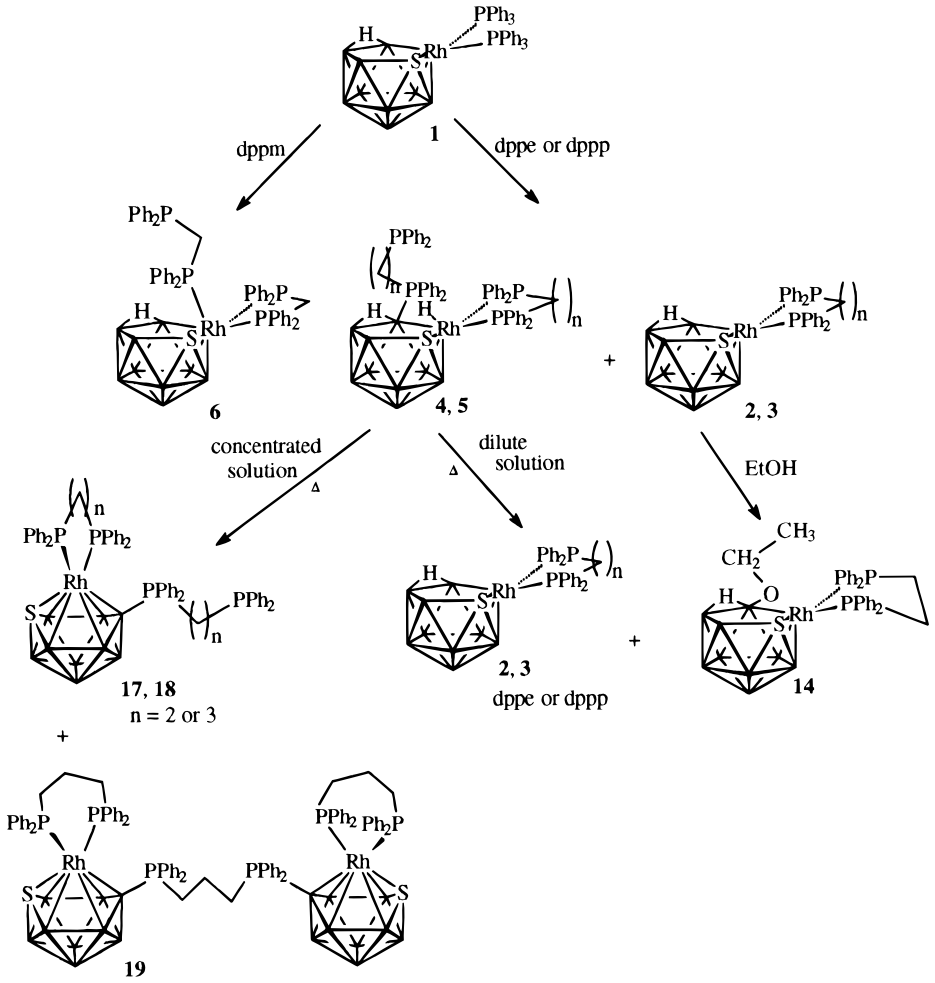

unsaturated rhodathiaborane chelates. At higher concentration, in competition with the dissociation, the adducts **4** and **5** also experience a *nido* to *closo* transformation, with loss of H_2, presumably the bridging H and Rh−H hydride atoms. The chemistry described herein is summarized in Scheme 2. Reactions of **1** with 1,*n*-bis(diphenylphosphino)alkanes have provided a route to the formation of new rhodathiaboranes containing pendant phosphine groups, PPh_2. These groups are reactive centers available for further chemistry. Facile oxidation with oxygen in solution has been observed at the pendant PPh_2 group for all the species. The unsaturated Rh center for compounds **3** and **14**, and the presence of the reactive PPh_2 group in **4**−**6**, **17**, and **18** perhaps account for our inability to obtain satisfactory elemental analyses for these compounds. The formation of the dicage derivative **19** demonstrates that an entrance to linked cages and thence possibly supramolecular chemistry are also available in this system. These and other aspects of the chemistry of compound **1** remain to be further developed. Some chemistry of the species **6** has been described in a preliminary communication.[20]

Experimental Section

General Considerations. Solvents used were reagent grade and were dried before use. Some reactions were carried out using a Schlenk line, a glovebox, and standard techniques for handling air-sensitive compounds.[27] Products were isolated in air using thin-layer chromatography (TLC) on 20 × 20 cm glass plates coated with 0.1 cm of silica gel (Aldrich standard grade with gypsum binder and fluorescent indicator), made from aqueous slurries followed by drying in air at 80 °C. [8,8-$(PPh_3)_2$-*nido*-8,7-$RhSB_9H_{10}$] (**1**) was prepared according to the literature method[14b] from the reaction between $Cs[SB_9H_{12}]$[28] and $[RhCl(PPh_3)_3]$.[29] PPh_3 and $[(PPh_2)_2(CH_2)_2]$ were obtained from Aldrich, and $[(PPh_2)_2(CH_2)]$ and $[(PPh_2)_2(CH_2)_3]$ were obtained from Strem. Solvents used were reagent grade and were dried before use. NMR spectroscopy was carried out on a Bruker ARX 500 spectrometer operating at 500.1 MHz for proton, 160.5 MHz for boron-11, and at 202.5 MHz for phosphorus-31 and on a Varian Unity Plus 300 spectrometer operating at 96.2 MHz for ^{11}B, 299.9 MHz for ^{1}H, and 121.4 MHz for ^{31}P. Chemical shifts are reported in ppm for $CDCl_3$ solutions, unless otherwise stated, to low field (high frequency) of $Et_2O{\cdot}BF_3$ for ^{11}B, of $SiMe_4$ for ^{1}H, and of 85% H_3PO_4 for ^{31}P. Elemental analyses were attempted by Atlantic Microlabs Inc., Norcross, GA, but they were unable to obtain satisfactory data; however, NMR spectra were run on all samples sent for mass spectra and crystal growth was generated from NMR samples, after spectral analysis. The mass spectra were measured in the FAB mode on a VG ZAB-E using 3-nitrobenzyl alcohol (3-NBA) and also on a Kratos MS-50 using 3-NBA/Ar gas, at the Washington University Mass Spectrometry Resource, an NIH Research Resource (Grant No. P41RR0954).

(27) Shriver, D. F.; Drezdon, M. A. *The Manipulation of Air-Sensitive Compounds*; Wiley: New York, 1986.
(28) Rudolph, R. W.; Pretzer, W. R. *Inorg. Synth.* **1983,** *22,* 226.
(29) Osborn, J. A.; Wilkinson, G. *Inorg. Synth.* **1990**, *28,* 77.

Preparation of [8,8-(η^2-dppe)-*nido*-8,7-RhSB$_9$H$_{10}$] (2). A route different from that reported[16] is described herein. A 50 mg (0.07 mmol) portion of [8,8-(PPh$_3$)$_2$-*nido*-8,7-RhSB$_9$H$_{10}$] was dissolved in 30 mL of CH_2Cl_2 in a 50 mL round-bottom flask; the resulting bright red solution was degassed and the system filled with nitrogen gas. Then dppe (28 mg, 0.07 mmol) was added to the reaction vessel at ambient temperature. Upon addition, the initially red solution turned immediately to orange. The reaction mixture was stirred at room temperature under N_2 for 16 h. After this time, the solvent was reduced in volume and the resulting orange solution applied to TLC plates using CH_2Cl_2−pentane (70:30) as mobile phase. The chromatogram resulted in the isolation of 32 mg of an orange air-stable solid with R_f 0.3, which was characterized as the previously reported 11-vertex rhodathiborane [8,8-(η^2-dppe)-*nido*-8,7-RhSB$_9$H$_{10}$] (**2**: 32 mg, 0.05 mmol; 71%). The NMR data conform to the values published in ref 16. ^{11}B NMR (160.5 MHz, $CDCl_3$, 300 K; ordered as relative intensity $\delta(^{11}B)$ (relative to $BF_3{\cdot}OEt_2$) [$\delta(^1H)$]): 3BH 10.8 [3.26, 2H; 2.34, 1H], 1BH −7.4 [1.92, 1H], 4BH −12.2 [2.88, 2H; 1.64, 2H], 1BH −27.0 [1.65] (^1J(B,H) coupling constants could not be resolved due to broadness of the peaks). Additional ^{1}H NMR (500 MHz, $CDCl_3$, 300 K): δ 7.69−7.25 (m, 20H; C_6H_5), 2.77 (br m, 2H; CH_2), 2.32 (br m, 2H; CH_2), −2.25 (br s, 1H; μ-H−BB). ^{31}P-{^{1}H} NMR (202.5 MHz, $CDCl_3$, 228 K): δ 66.1 (dd, ^1J(Rh,P) = 142 Hz, ^1J(P,P) = 25 Hz), 49.9 (dd, ^1J(Rh,P) = 133 Hz).

Reaction of [8,8-(PPh$_3$)$_2$-*nido*-8,7-RhSB$_9$H$_{10}$] with {(CH$_2$)$_2$(PPh$_2$)$_2$] (dppe). A 50 mL two-neck round-bottom flask was loaded with 168 mg (0.22 mmol) of [8,8-(PPh$_3$)$_2$-*nido*-8,7-RhSB$_9$H$_{10}$] and 30 mL of CH_2Cl_2; the system was filled with nitrogen and evacuated several times. Then dppe 263 mg (0.66 mmol) was added via a tip tube previously attached to the reaction vessel. The initial bright red solution of the rhodathiaborane turned orange upon the addition of the phosphine. The reaction mixture was stirred for 25 h. After this time, the solvent was evaporated to dryness, the orange residue dissolved in CH_2Cl_2−pentane, and this solution applied to TLC plates. The chromatogram was developed using CH_2Cl_2−pentane (70:30) as eluent. Two yellow components were separated from the plates with R_f values of 0.1 and 0.3, which were characterized as [8,8-(η^2-dppe)-9-(η^1-dppe)-*nido*-8,7-RhSB$_9$H$_{10}$] (**4**: 38 mg, 0.04 mmol; 18%) and [8,8-(η^2-dppe)-*nido*-8,7-RhSB$_9$H$_{10}$] (**2**: 52 mg; 0.08 mmol; 36%), respectively. The new rhodathiaborane [8,8-(η^2-dppe)-9-(η^1-dppe)-*nido*-8,7-RhSB$_9$H$_{10}$] (**4**) is unstable in solution, and it reacts further, giving rise to the *closo* derivative [1,1-(η^2-dppe)-3-(η^1-ddpe)-1,2-RhSB$_9$H$_8$] (**17**). The dangling phosphine group, present in these species, reacts with oxygen in solution, giving rise to the P═O derivative [1,1-(η^2-dppe)-3-(η^1-ddpeO)- *closo*-1,2-RhSB$_9$H$_8$] (**20**), studied by X-ray diffraction analysis.

[8,8-(η^2-dppe)-9-(η^1-dppe)-*nido*-8,7-RhSB$_9$H$_{10}$] (4). ^{11}B NMR (160.5 MHz, $CDCl_3$, 300 K; ordered as relative intensity $\delta(^{11}B)$ (relative to $BF_3{\cdot}OEt_2$) [$\delta(^1H)$]): 1BH 2.2 [3.40], 1BH −1.4 [2.92], 4B −5.8 [2.52, 1H; 2.34, 2H], 2BH −20.2 [1.63, 1.37], 1BH −25.5 [1.53] (^1J(B,H) coupling constants could not be resolved due to broadness of the peaks). Additional ^{1}H NMR (500 MHz, $CDCl_3$, 300 K): δ 7.85−6.78 (m, 40H; C_6H_5), 2.65 (apparent d, J = ca. 44 Hz, 2H; CH_2), 2.29−2.07 (br m, 4H; CH_2), 1.80 (br m, 2H; CH_2), −1.39 (s, 1H; μ-H−BB), −11.97 (m, 1H; RhH). ^{31}P{^{1}H} NMR (202.5 MHz, $CDCl_3$, 300 K): δ 58.1 (br d, ^1J(Rh,P) not well resolved; 1P), 54.7 (d, ^1J(Rh,P) = 123 Hz, 1P), 5.9 (v br, 1P; Ph_2PB), −12.4 (d, ^3J(P,P) = 34 Hz, 1P; dangling PPh$_2$). Mass spectral data for **4** (LRMS, VG ZAB-SE, FAB+ with 3-NBA; amu): calcd maximum for [(MO − H$_2$) + H]$^+$ $C_{52}H_{57}B_9OP_4RhS$, 1054.3; obsd, 1054.2. The mass envelope for the measured masses for **4** matches that calculated from the known isotopic abundances of the constituent elements. The data are available as Supporting Information.

[1,1-(η^2-dppe)-3-(η^1-ddpe)-*closo*-1,2-RhSB$_9$H$_8$] (17). ^{11}B NMR (160.5 MHz, $CDCl_3$, 300 K; ordered as relative intensity $\delta(^{11}B)$ (assignments) (relative to $BF_3{\cdot}OEt_2$) [$\delta(^1H)$]): 1B(3) 34.9 [B−PPh$_3$], 1BH(9) 27.6 [4.02, d, J = 14 Hz], 3BH(4,5; 8) 2.0 [2.94, 1H; 2.12, 2H], 2BH(6,7) −15.8 [0.57], 2BH(10,11) −27.4 [0.16] (^1J(B,H) coupling constants could not be resolved due to broadness of the peaks). Additional ^{1}H NMR (500 MHz, $CDCl_3$, 300 K): δ 7.47−7.06 (m, 40H; C_6H_5), 2.47−2.42 (br m, 2H; CH_2), 2.30−2.27 (m, 2H; CH_2), 2.20−2.16 (m, 2H; CH_2), 1.84−1.80 (m, 2H; CH_2). ^{31}P{^{1}H} NMR (202.5 MHz, $CDCl_3$, 300 K): δ 61.3 (d, ^1J(Rh,P) = 148 Hz, 2P), 4.9 (v br; PPh$_2$B), −12.8 (d, ^3J(P,P) = 39 Hz; dangling PPh$_2$).

[1,1-(η^2-dppe)-3-(η^1-dppeO)-*closo*-1,2-Rh$_5$B$_9$H$_8$] (20). ^{11}B NMR (96.2 MHz, $CDCl_3$, 300 K; ordered as relative intensity $\delta(^{11}B)$ (relative to $BF_3{\cdot}OEt_2$) [$\delta(^1H)$]): 1B(3) 33.6 (d, ^1J(P,B) = 114 Hz), 1BH(9) 27.2 [4.08, d, J = 17 Hz], 3BH(4,5; 8) 1.23 [2.97, 1H; 2.13, 2H], 2BH(6,7) −15.8 [0.68], 2BH(10,11) −27.3 [0.23] (^1J(B,H) coupling constants could not be resolved due to broadness of the peaks; assignments were made by comparison with *closo* analogues previously reported).[14b] Additional ^{1}H NMR (500 MHz, $CDCl_3$, 300 K): δ 7.63−6.86 (m, 40H; C_6H_5), 2.57 (m. 4H; CH_2), 2.26−2.19 (m, 4H; CH_2). ^{31}P-{^{1}H} NMR (202.5 MHz, $CDCl_3$, 300 K): δ 61.2 (d, ^1J(Rh,P) = 149 Hz, 2P), 31.9 (d, ^3J(P,P) = 45 Hz, 1P; PPh$_2$O), 2.3 (v br, 1P; PPh$_2$−B). LRMS (VG ZAB-E, FAB with 3-NBA/Gly/TFA; amu): calcd maximum for $C_{52}H_{56}B_9OP_4RhS$ [MO]$^+$, 1053.3; obsd 1053.7. The mass envelope for the measured masses for **17** matches that calculated from the known isotopic abundances of the constituent elements. The data are available as Supporting Information.

Preparation of [8,8-(η^2-dppp)-*nido*-8,7-RhSB$_9$H$_{10}$] (3). A 62 mg (0.08 mmol) portion of [8,8-(PPh$_3$)$_2$-*nido*-8,7-RhSB$_9$H$_{10}$] (**1**) was dissolved in 25 mL of CH_2Cl_2. The reaction system was evacuated and filled with nitrogen; then 34 mg (0.08 mmol) of dppp was added to the reaction flask. The resulting orange solution was stirred at room temperature under N_2 for 25 h. The final reaction mixture was reduced in volume and applied to TLC plates using CH_2Cl_2−pentane (3:2). A yellow band with R_f 0.7 was removed from the TLC plates, and the component was extracted from the silica gel using CH_2Cl_2 solvent. Recrystallization in CH_2Cl_2−pentane gave rise to the isolation of 46 mg of a yellow product, which was characterized as [8,8-(η^2-dppp)-*nido*-8,7-RHSB$_9$H$_{10}$] (**3**; 0.07 mmol, 88%). ^{11}B NMR (160.5 MHz, $CDCl_3$, 231 K; ordered as relative intensity $\delta(^{11}B)$ (relative to $BF_3{\cdot}OEt_2$) [$\delta(^1H)$]): 1BH 15.0 [3.64], 1BH 7.9 [3.20], 3BH 1.7 [3.02, 2.36, 1.82], 1BH −8.5 [1.97], 3BH −24.1 [1.43, 1.24, 0.76] (^1J(B,H) coupling constants could not be resolved due to broadness of the peaks). Additional ^{1}H NMR (500 MHz, $CDCl_3$, 231 K): δ 7.42−7.16 (m, 20H; C_6H_5), 2.71−2.64 (br m, 2H; Ph_2PCH_2), 2.64−2.56 (br m, 3H; Ph_2PCH_2CHH), 1.85−1.73 (m, 1H; Ph_2PCH_2CHH), −2.02 (s, 1H; μ-H−BB). ^{31}P{^{1}H} NMR (202.5 MHz, $CDCl_3$, 231 K): δ 22.5 (dd, ^1J(Rh,P) = 140 Hz, ^2J(P,P) = 55 Hz), 6.9 (dd, ^1J(Rh,P) = 130 Hz); the two doublet of doublets coalesce at 310 K ($\Delta G^{\ddagger}$ = 53 kJ mol^{-1}). ^{11}B NMR (160.5 MHz, $CDCl_3$, 331 K; ordered as relative intensity $\delta(^{11}B)$ (relative to $BF_3{\cdot}OEt_2$) [$\delta(^1H)$]): 3BH 10.1 [3.37, 1H; 2.9, 2H], 1BH −7.9, ^1J(B,H) = 140 Hz, [2.07], 4BH −10.6 [2.25, 2H; 1.70, 2H], 1BH −26.7 [1.52]. Additional ^{1}H NMR (500 MHz, $CDCl_3$, 331 K): δ 7.50−7.18 (m, 20H; C_6H_5), 2.66 (m, 2H; Ph_2PCH_2), 2.53 (m, 2H; Ph_2PCH_2), 1.67 (m, 1H; $Ph_2PCH_2CH_2$), −1.80 (s, 1H; μ-H−BB). ^{31}P{^{1}H} NMR (202.5 MHz, $CDCl_3$, 331 K): δ 14.8 (v br, coupling no resolved). LRMS (VG ZAB-E (in FAB mode with 3-NBA; amu): calcd for [$C_{27}H_{36}B_9P_2RhS$]$^+$, 654.8; obsd, cluster at 641−657 overlapped with spectral noise, precluding a detailed comparison.

Reaction of [8,8-(PPh$_3$)$_2$-*nido*-8,7-RHSB$_9$H$_{10}$] with [(CH$_2$)$_3$PPh$_2$)$_2$] (dppp). A 50 mg (0.065 mmol) portion of [8,8-(PPh$_3$)$_2$-*nido*-8,7-RhSB$_9$H$_{10}$] (**1**) was placed in a two-neck 50 mL round-bottom flask and dissolved in 20 mL of CH_2Cl_2. The system was evacuated and filled with nitrogen. To the resulting bright red solution of the rhodathiaborane was added 82 mg (0.20 mmol) of dppp via a sidearm of the reaction vessel. The initial bright red solution immediately turned yellow on

the addition of phosphine. The reaction mixture was stirred at ambient temperature under N_2 for 16 h. After this time, the final yellow solution was reduced in volume and applied to TLC plates, using CH_2Cl_2−pentane (3:2) as eluent. The chromatogram resulted in the isolation of two compounds, which were characterized as the yellow [8-(η^2-dppp)-*nido*-8,7-$RhSB_9H_{10}$] (**3**: R_f 0.41; 20 mg, 0.03 mmol; 47%) and the yellow [8-(η^2-dppp)-9-(η^1-dppp)-*nido*-8,7-$RhSB_9H_{10}$] (**5**: R_f 0.18; 30 mg, 0.03 mmol; 46%).

[8,8-(η^2-dppp)-9-(η^1-dppp)-*nido*-8,7-$RhSB_9H_{10}$] (5). ^{11}B NMR (160.5 MHz, $CDCl_3$, 300 K; ordered as relative intensity δ(^{11}B) (relative to BF_3·OEt_2) [δ(^{1}H)]): 2BH 4.6 [3.54; 3.08, d, J = 15 Hz], 1BH −0.1 [2.25], 1BH −2.9 [2.72], 1BH −6.4 [B−PPh_2], 1BH −8.6 [2.12], 2BH −16.7 [1.44], 1BH −23.9 [1.50] (^1J(B,H) coupling constants could not be resolved due to broadness of the peaks). Additional ^{1}H NMR (500 MHz, $CDCl_3$, 300 K): δ 7.50−6.93 (m, 40H; C_6H_5), 2.68 (br m, 2H; CH_2), 2.53 (br m, 2H; CH_2), 2.16 (br m, 2H; CH_2), 2.04 (br m, 2H; CH_2), 1.92 (br m, 2H; CH_2), 1.83 (m, 2H; CH_2), −2.39 (s, 1H; μ-*H*−BB), −11.96 (m, J = ca. 10 Hz; {^{31}P}, d, ^1J(H,Rh) = 18 Hz). ^{31}P{^{1}H} NMR (203 MHz, $CDCl_3$, 300 K): δ 13.6 (br dd, ^1J(P,Rh) = ca. 108 Hz), 9.3 (dd, ^1J(P,Rh) = 119 Hz, ^1J(P,P) = 44 Hz), 7.4 (v br; PPh_2P−B), −18.8 (s, dangling PPh_2P). LRMS (VG ZAB-E (in FAB+ mode with Gly/thioglycerol-Na; amu): calcd for $C_{54}H_{62}P_4B_9RhS$, 1067.35; obsd, 1067.2; calcd maximum for $C_{54}H_{62}P_4B_9RhSO$ [M + O]$^+$, 1083.35; obsd, 1082.2. The mass spectral envelopes for the measured masses for both **5** and **5′** [M + O]$^+$ match those calculated from the known isotopic abundances of the constituent elements. The data are available as Supporting Information.

Preparation of [8,8-(η^2-dppm)(η^1-dppm)-*nido*-8,7-$RhSB_9H_{10}$] (6). (a) dppm (30 mg, 0.078 mmol) was added slowly to a solution of [8,8-$(PPh_2)_2$-*nido*-7,8-$RhSB_9H_{10}$] (**1**; 60 mg, 0.078 mmol) in CH_2Cl_2 under N_2. The reaction mixture was stirred at room temperature for 1 h. After this time, the solvent was reduced in volume and the solution applied to a TLC plate, with CH_2Cl_2−pentane (3:2) as the mobile phase. A compound with R_f 0.4 was isolated and characterized as [8-(η^2-dppm)-8-(η^1-dppm)-*nido*-7,8-RhB_9H_{10}] (25 mg, 0.025 mmol, 32%).

(b) To a solution of [8,8-$(PPh_2)_2$-*nido*-7,8-$RhSB_9H_{10}$] (32 mg, 0.042 mmol) in CH_2Cl_2 was added dppm (51 mg, 0.133 mmol). The initial bright red solution turned immediately to bright yellow; this reaction mixture was stirred at room temperature under nitrogen. After 40 min, the solvent was evaporated under vacuum and the yellow residue applied to TLC using a CH_2Cl_2−pentane (3:2) mixture as the mobile phase. The chromatogram allowed separation of a yellow component with R_f 0.4, which was characterized as [8-(η^2-dppm)-8-(η^1-dppm)-*nido*-7,8-RhB_9H_{10}] (**6**: 20 mg, 0.02 mmol; 47%). ^{11}B NMR (160.5 MHz, $CDCl_3$, 300 K; ordered as relative intensity δ(^{11}B) (relative to BF_3·OEt_2) [δ(^{1}H)]): 1BH 14.7 [3.85], 3BH 8.1 [2.83, d, J = 12 Hz; 3.27, d, J = 23 Hz; 3.74], 1.2 [2.11], 1BH −13.5 [1.68], 1BH −14.9 [1.68], 1BH −19.0 [1.71], 1BH −29.2 [1.10]. Additional ^{1}H NMR (500 MHz, $CDCl_3$, 300 K): δ 7.80−6.52 (m, 40H; C_6H_5), −4.38 (s, 1H; μ-H). ^{1}H{^{31}P} NMR (500 MHz, CD_2Cl_2, 25 °C): δ 4.29, 4.18 (both AB q, ^2J(H,H) = 14 Hz, 2H; CH_2), 3.58, 2.83 (each d, ^2J(H,H) = 16 Hz, 2H; CH_2). ^{31}P NMR (202.5 MHz, CD_2Cl_2, 25 °C): δ 15.2 (dt, ^1J(P,Rh) = 126 Hz, ^2J(P,P) = 26 Hz), −7.7 (ddd, ^1J(P,Rh) = 122 Hz, ^2J(P,P) = 13 and 63 Hz), −26.9 (d, ^2J(P,P) = 31 Hz), −42.9 (br td, ^1J(P,Rh) + ^2J(P,P) = ca. 68 Hz, ^2J(P,P) = ca. 26 Hz). HRMS (FAB Kratos MS-50, 3-NBA/Ar gas; amu): calcd for $C_{50}H_{52}B_9P_4RhS$, 1010.2633, [M$^+$ − H_2]; found, 1010.2632.

Reaction of [8,8-(η^2-dppp)-nido-8,7-$RhSB_9H_{10}$] (3) with EtOH. A 14 mg (0.021 mmol) portion of [8-(η^2-dppp)-*nido*-8,7-$RhSB_9H_{10}$] (**1**) was dissolved in 20 mL of CH_2Cl_2−EtOH (1:1). The resulting yellow-orange solution was degassed, the system filled with nitrogen, and the reaction mixture stirred at room temperature under nitrogen for 2 days. After this time, the solution was evaporated to dryness, the orange residue dissolved in the minimum amount of CH_2Cl_2, and the solution applied to TLC plates. The plates were developed using CH_2Cl_2−pentane (7:3) as the mobile phase. Two compounds were separated and identified as unreacted [8-(η^2-dppp)-*nido*-8,7-$RhSB_9H_{10}$] (**3**: R_f 0.63) and [8-(η^2-dppp)-9-(OEt)-*nido*-8,7-$RhSB_9H_{10}$] (**14**: R_f 0.75; 8 mg, 55%).

[8,8-(η^2-dppp)-9-(OEt)-*nido*-8,7-$RhSB_9H_9$] (14). ^{11}B NMR (160.5 MHz, $CDCl_3$, 300 K; ordered as relative intensity δ-(^{11}B) (relative to BF_3·OEt_2); ^1J(B,H) [δ(^{1}H)]): 1B 26.6 [OEt], 1BH 14.2 [3.58], 1BH 4.5 [2.18], 1BH −5.1, br d, 123 Hz, [2.22, d, J = 20 Hz], 1BH −9.8 [2.33], 1BH −10.3, br d, ca. 116 Hz [2.32], 1BH −24.9, d, 144 Hz [1.24], 1BH −30.4 [1.20], 1BH −31.7, d, 122 Hz [0.40] (not all ^1J(B,H) coupling constants could be resolved due to broadness of the peaks). Additional ^{1}H NMR (500 MHz, $CDCl_3$, 300 K): δ 7.69−7.12 (m, 20H; C_6H_5), 4.11−4.05 (m, 1H; OC*H*HCH_3), 4.02−3.96 (m, 1H; OC*H*HCH_3), 2.81−2.74 (br m, 1H; Ph_2PCHH), 2.63−2.54 (br m, 3H; $Ph_2PCHHCH_2CH_2PPh_2$), 2.49−2.36 (v br m, 1H; Ph_2-$PCH_2CHHCH_2PPh_2$), 1.83−1.72 (br m, 1H; $Ph_2PCH_2CHHCH_2$-PPh_2), 1.50 (t, ^3J(H,H) = 7 Hz, 3H; OCH_2CH_3), −0.82 (s, 1H; μ-*H*BB). ^{31}P{^{1}H} NMR (121.4 MHz, $CDCl_3$, 300 K): δ 25.8 (dd, ^1J(Rh,P) = 151 Hz, ^2J(P,P) = 55 Hz), 7.7 (dd, ^1J(Rh,P) = 130 Hz). These two peaks do not coalesce at 373 K in $C_6D_5CD_3$, implying a $\Delta G^{\ddagger}$ value higher than 64 kJ mol^{-1} for the fluxional process. LRMS (VG ZAB-E in FAB+ ONPOE; amu): calcd for [$C_{29}H_{40}B_9P_2ORhS$]$^+$, 698.84; obsd, 699.1. The mass envelopes for the measured masses for **14** match quite well with those calculated from the known isotopic abundances of the constituent elements, although the spectra were quite noisy and overlapped features from the [M + Li]$^+$ cluster and other unidentifiable features. The mass spectral data are all included as Supporting Information.

[8,8-(η^2-dppp)-8-(CH_3CN)-*nido*-8,7-$RhSB_9H_{10}$] (21) was formed in quantitative yield on refluxing [8,8-(η^2-dppp)-*nido*-8,7-$RhSB_9H_{10}$] **(3)** in CH_3CN. Compound **3** is insoluble in CH_3-CN, but the yellow solid dissolved on reflux to afford a bright yellow solution from which yellow crystals were obtained. The species was amenable to X-ray diffraction analysis, which afforded data comparable to those for the related species [8,8-(η^2-dppe)-8-(CH_3CN)-*nido*-8,7-$RhSB_9H_{10}$] reported by Welch et al.[16] The data have been deposited with the Cambridge Crystallographic Data Center as supplementary publication No. 133103.

Thermolysis of [8,8-(η^2-dppe)-9-(η^1-dppe)-*nido*-8,7-$RhSB_9H_{10}$] (4) and [8,8-(η^2-dppp)-9-(η^1-dppp)-*nido*-8,7-$RhSB_9H_{10}$] (5). (a) In a 50 mL round-bottom flask, 7 mg of [8-(η^2-dppp)-9-(η^1-dppp)-*nido*-8,7-$RhSB_9H_{10}$] (**5**) was dissolved in 30 mL of CH_2Cl_2. The solution was degassed and, then, heated at reflux temperature under N_2 for 6 days. After this time, NMR spectroscopy showed that the *nido*-rhodathiaborane had transformed quantitatively into [8-(η^2-dppp)-*nido*-8,7-$RhSB_9H_{10}$] (**3**) and free dppp. Under the same conditions, thermolysis of [8-(η^2-dppe)-9-(η^1-dppe)-*nido*-8,7-$RhSB_9H_{10}$] (**4**) afforded a mixture of [1-(η^2-dppe)-3-(η^1-dppe)-*closo*-1,2-$RhSB_9H_8$] (**17**), [8-(η^2-dppe)-*nido*-8,7-$RhSB_9H_{10}$] (**2**), and free dppe. In this mixture, the *nido*-rhodathiaborane and free phosphine were the major components.

(b) In a 5 mm NMR tube, 7 mg of [8-(η^2-dppp)-9-(η^1-dppp)-*nido*-8,7-$RhSB_9H_{10}$] (**5**) was dissolved in $CDCl_3$ (ca. 0.8 mL) and, then, heated to 40 °C under air atmosphere for 1 day. ^{31}P NMR spectra of the crude reaction mixture indicated a mixture of species, which were separated by TLC, using CH_2Cl_2−pentane (3:1). The chromatogram resulted in the isolation of [8-(η^2-dppp)-*nido*-8,7-$RhSB_9H_{10}$] (**3**: R_f 0.7; 46%), [{1,1-(η^2-dppp)-*closo*-1,2-$RhSB_9H_8$}$_2$-3,3′-μ-(dppp)] (**19**: R_f 0.3; 36%), and [1,1-(η^2-dppp)-3-(η^1-ddppO)-*closo*-1,2-$RhSB_9H_8$] (**18**: R_f 0.0; 14%), together with free dppp. Under the same conditions, thermolysis of 7 mg of [8,8-(η^2-dppe)-9-(η^1-dppe)-*nido*-8,7-$RhSB_9H_{10}$] (**4**) gives rise to a mixture of [8,8-(η^2-dppe)-*nido*-8,7-$RhSB_9H_{10}$] (**2**), [1,1-(η^2-dppe)-3-(η^1-ddpeO)-*closo*-1,2-$RhSB_9H_8$] (**20**), and free dppe, the *closo*-rhodathiaborane being the major component of the resulting mixture.

[{1,1-(η^2-dppp)-*closo*-1,2-$RhSB_9H_8$}$_2$-3,3′-μ-(dppp)] (19). ^{11}B NMR (160.5 MHz, $CDCl_3$, 300 K; ordered as relative intensity $\delta(^{11}B)$ (relative to $BF_3{\cdot}OEt_2$) [$\delta(^1H)$]): 1BH 32.1 [Ph_2-PB], 1BH 25.7 [4.03], 3BH 1.6 [2.24, 2H; 2.98, 1H], 2BH −17.6 [-0.04], 2BH −27.9 [0.29] (^1J(B,H) coupling constants could not be resolved due to broadness of the peaks). Additional ^{1}H NMR (500 MHz, $CDCl_3$, 300 K): δ 7.70−6.90 (m, 60H; C_6H_5), 2.16−2.00 (br m, 18; H; CH_2). $^{31}P\{^1H\}$ NMR (202.5 MHz, $CDCl_3$, 300 K): δ 14.7 (d, ^1J(Rh,P) = 140 Hz; 4P), 1.81 (v br, 2P; Ph_2PB). LR-MS for **19** (ZAB-E, FAB+ with 3-NBA; amu): calcd maximum for $C_{81}H_{94}B_{18}P_6Rh_2S_2$, [M$^+$], 1718.5; obsd, 1718.3. The mass envelopes for the measured masses for **19** match quite well with those calculated from the known isotopic abundances of the constituent elements. The data are available as Supporting Information.

[1,1-(η^2-dppp)-3-(η^1-ddppO)-*closo*-1,2-$RhSB_9H_8$] (18). ^{11}B NMR (160.5 MHz, $CDCl_3$, 300 K; ordered as relative intensity $\delta(^{11}B)$ (relative to $BF_3{\cdot}OEt_2$) [$\delta(^1H)$]): 1BH 32.5 [Ph_2PB], 1BH 25.8 [3.88], 3BH 1.6 [2.18, 2H; 2.79, 1H], 2BH −17.8 [−0.16], 2BH −32.9 [0.07] (^1J(B,H) coupling constants could not be resolved due to broadness of the peaks). Additional ^{1}H NMR (500 MHz, $CDCl_3$, 300 K): δ 7.77−6.97 (m, 40H; C_6H_5), 2.77 (m, 2H; CH_2), 2.49 (m, 2H; CH_2), 2.01 (m, 2H; CH_2), 1.66 (m, 2H; CH_2). $^{31}P\{^1H\}$ NMR (202.5 MHz, $CDCl_3$, 300 K): δ 32.7 (s; $Ph_2P{=}O$), 14.0 (d, ^1J(Rh,P) = 141 Hz; 2P), 2.2 (v br, 1P; Ph_2PB). LRMS (VG ZAB-E, FAB+ with 3-NBA; amu): calcd for $C_{54}H_{60}B_9OP_4RhS$, i.e., [M + O]$^+$, 1081.4; obsd, 1081.3. The mass envelopes for the measured masses for **18** match quite well with those calculated from the known isotopic abundances of the constituent elements. The data are available as Supporting Information.

X-ray Diffraction Analysis for 3, 14, 6, 20, and 21. Crystals of appropriate dimensions were mounted on glass fibers in random orientations. Preliminary examinations and data collections were performed using a Bruker SMART charge coupled device (CCD) detector system single-crystal X-ray diffractometer using graphite-monochromated Mo Kα radiation (λ = 0.710 73 A) equipped with a sealed-tube X-ray source at −50 °C. Preliminary unit cell constants were determined with a set of 45 narrow frames (0.3° in ϖ) scans. A typical data set collected consists of 4028 frames of intensity data collected with a frame width of 0.3° in ϖ and counting time of 15 s/frame at a crystal to detector distance of 4.930 cm. The double-pass method of scanning was used to exclude any noise. The collected frames were integrated using an orientation matrix determined from the narrow frame scans. SMART and SAINT software packages[30] were used for data collection and data integration. Analysis of the integrated data did not show any decay. Final cell constants were determined by a global refinement of *xyz* centroids of 8192 reflections. Collected data were corrected for systematic errors using SADABS[31] based upon the Laue symmetry using equivalent reflections.

(30) Bruker Analytical X-ray Division, Madison, WI, 1997.

Crystal data and intensity data collection parameters are listed in Table 1. Structure solution and refinement were carried out using the SHELXTL-PLUS software package.[32] The structures were solved by direct methods and refined successfully in the space groups $P2_1/n$, $P\bar{1}$, $P\bar{1}$, and $P2_1/n$ for **3**, **14**, **6**, and **20**, respectively. Full-matrix least-squares refinement was carried out by minimizing $\sum w(F_o^2 - F_c^2)^2$. The non-hydrogen atoms were refined anisotropically to convergence. The hydrogen atoms were treated using an appropriate riding model (AFIX m3). The cage hydrogens were located from the difference Fourier and were refined. The final residual values $R(F)$ and $R_w(F^2)$ and the structure refinement parameters are listed in Table 1. The geometrical parameters are listed in Tables 2−5, and projection views of the molecules with non-hydrogen atoms represented by 50% probability ellipsoids, showing the atom labeling, are presented in Figures 1−3 and 6, respectively, for **3**, **14**, **6**, and **20**.

Complete listings of the atomic coordinates for the non-hydrogen atoms, the positional and isotropic displacement coefficients for hydrogen atoms, anisotropic displacement coefficients for the non-hydrogen atoms, and calculated and observed structure factors have been submitted as Supporting Information.

Acknowledgment. We acknowledge support from the Missouri Research Board, the donors of the Petroleum Research Fund, administered by the American Chemical Society, and the National Science Foundation. We also acknowledge the NSF (Grant No. CHE-9318696), the DOE (Grant No. DE-FG02-92CH10499), and the UM-St. Louis Center for Molecular Electronics for grants which allowed purchase of the Varian Unity Plus NMR spectrometer and the last two along with the NSF (Grant No. CHE-9309690) for funds to purchase the X-ray diffractometer. We thank the Washington University Mass Spectrometry NIH Research Resource (Grant No. P41RR094) for the mass spectra.

Supporting Information Available: Tables giving X-ray structural data for **3, 6, 14**, and **20,** including a summary of crystallographic parameters, atomic coordinates, bond distances and angles, and anisotropic thermal parameters, and tables giving detailed mass spectral data, including comparisons of the observed and calculated intensities of the parent peak envelope, for **3, 4, 5, 5′, 14, 17, 18, 19,** and **20**. This material is available free of charge via the Internet at http://pubs.acs.org.

OM9901168

(31) Blessing, R. H. *Acta Crystallogr.* **1995**, *A51*, 33.
(32) Sheldrick, G. M. Bruker Analytical X-ray Division, Madison, WI, 1997.